Important Notice to Authors

Attached is a proof copy of your forthcoming article in *Physical Review E*. The Article ID is **XH10025E**.

To print the pdf proof full size, be sure that you have not selected the "fit to page" option.

Your paper will be in the following section of the journal: Articles

Figures submitted electronically as separate PostScript files containing color usually appear in color in the online journal. However, all figures will appear in the print journal in black and white if you have not requested color-in-print reproduction and paid the applicable charges for color figures. For figures that will be color online but grayscale in print, please insure that the text and caption clearly describe the figure to readers who view it only in black and white.

No further publication processing will occur until we receive your response to this proof.

Questions and Comments to Address

Your article has 10 pages.

The numbered items below correspond to numbers in the margin of the proof pages pinpointing the source of the question and/or comment. The numbers will be removed from the margins prior to publication.

1 Changed access to accessibility. Please check for meaning. OK as done?
2 Please editing of time "2 h, 45 min". OK as done?
3 Changed "(see further)" to "(see later in the article)". OK as done?
4 Changed "plain symbols" to "solid symbols" (after "large symbols in Fig. 6"). OK as done?
5 Combined Supplemental Material references into one reference [4], deleted others, and reordered citations and reference list to match. OK as done?
6 Please provide volume number, if applicable, for Ref. [17].

Other Items to Check

- Please check your title, author list, receipt date, and PACS numbers. More information on PACS numbers is available online at http://publish.aps.org/PACS/.
- Please proofread the article very carefully.
- Please check that your figures are accurate and sized properly. Figure quality in this proof is the quality to be used in the online journal. To achieve manageable file size for online delivery, some compression and downsampling of figures may have occurred. Fine details may have become somewhat fuzzy, especially in color figures. The print journal uses files of higher resolution and therefore details may be sharper in print. Figures to be published in color online will appear in color on these proofs if viewed on a color monitor or printed on color printer.

Ways to Respond

- ***Web:*** If you accessed this proof online, follow the instructions on the web page to submit corrections.
- ***Email:*** Send corrections
  To: preproofs@aptaracorp.com
  Subject: **XH10025E** proof corrections
- ***Fax:*** Return this proof with corrections to +1.703.204.4619. Write **Attention:** PRE Project Manager and the Article ID, **XH10025E**, on the proof copy unless it is already printed on your proof printout.
- ***Mail:*** Return this proof with corrections to **Attention:** PRE Project Manager, Physical Review E, c/o Aptara, 3110 Fairview Park Drive, Suite #900, Falls Church, VA 22042-4534, USA.

PHYSICAL REVIEW E **00**, 001300 (2012)

How does an ice block assembly melt?

S. Dorbolo,[1] F. Ludewig,[2] N. Vandewalle,[2] and C. Laroche[3]
[1]*FNRS, GRASP, Physics Department, University of Liège, B-4000 Liège, Belgium*
[2]*GRASP, Physics Department, University of Liège, B-4000 Liège, Belgium*
[3]*Private Laboratory, 39 rue de la Madeleine, F-69007 Lyon, France*
(Received 24 August 2011; revised manuscript received 22 February 2012; published xxxxx)

The melting of an assembly of ice blocks contained in a vertical cylinder and under an unidirectional load was investigated. The total volume occupied by the ice blocks and the volume of ice were simultaneously measured which allowed one to determine the volume fraction of the ice in the cylinder. While the ice volume continuously decreases, sudden breakdowns of the total volume were observed. Large reorganizations of the whole assembly occur. However, the maximal volume fraction found just after a large reorganization decreased with time. In addition, the modifications of the pile structure were investigated using an x-ray tomography imaging before and after one collapse. As the packing is better ordered along the walls, we suggest that the motion of the piston is governed by the layer of ice blocks located along the container wall. This layer was modeled by a two-dimensional assembly of disks. The model supports the idea that the geometrical frustrations explain the dynamics of the successive reorganization due to the shrinkage of the grains. Finally, numerical simulations allow one to conclude that the dynamics of the melting of the ice blocks is governed (i) by the confinement effect which induces defects in the packing and (ii) by the low friction between the ice blocks.

DOI: 10.1103/PhysRevE.00.001300 PACS number(s): 81.05.Rm, 45.70.Cc, 64.70.dj

I. INTRODUCTION

When an assembly of spherical noncohesive grains is poured into a vessel, the volume occupied by the grains is a very debated subject since Kepler's conjecture in 1611. Even after the last two decades of intensive research in granular materials, the problem remains an open question [1,2]. The macroscopic value that reflects the volume occupied by the grains is the volume fraction η, defined as the ratio between the volume of the grains and the volume occupied by the whole grain assembly. The ingredients that determine the volume fraction of the pile are due to the geometrical and to the mechanical constraints. Each grain is to reach a stable position which is determined by the geometry of its neighborhood. More precisely, a grain is stable either when at least three contacts are established below its gravity center or when grain-grain friction is sufficient to stop the grain. The geometrical frustration and the friction are responsible for arching and a so-called jamming of the pile [2,3]. Indeed, the potential energy of the pile, given by the sum of all the potential energies of the grains, is a local minimum of the energy in the configuration space. A bead assembly contained in a box may be assimilated to a glassy state [5]. Besides the friction between grains, the shape of the grains is relevant for determining the volume fraction of a packing. Since the seminal work by Donev *et al*. on the packing of ellipsoids [6,7], the volume fraction of more complex grains has been investigated like Platonic solids [8].

Even more interesting is the manner to increase the volume fraction (to increase the density) by tapping [9–12], by shaking [13], by shearing [14,15], by thermal cycling [16], by moving an intruder [17]. Generally speaking, the method consists of breaking the contact network and then allowing a reorganization that may conduct to a highest volume fraction. This process is complex. For example, from one tap to another, the potential energy of the pile jumps from one local minimum to another characterized, maybe, by a higher volume fraction.

In this work, we envisaged a particular granular material that was made of ice blocks. The ice grains (blocks) were placed in a vessel at room temperature and under a mechanical vertical compression. Basically, an assembly of ice blocks was placed in a piston. During the melting of the ice blocks, the piston went down because the size and shape of the grains continuously change. Consequently, the contact geometry, the contact network, and the force network were dynamical and kept on changing. The natural question concerns the evolution of the volume fraction: Does the volume fraction increase or decrease during the melting of the ice blocks? Moreover, as the grains are melting, the assembly becomes more and more fragile. Large reorganizations are supposed to be observed which must conduct to a packing which is robust enough to sustain the load.

Ice blocks are particularly advantageous for our purpose: (i) As the blocks were immersed, the ice grains are not cohesive. Note that a recent paper approaches cohesive ice grains [18]. (ii) The coefficient of friction between two melting ice blocks is very low, about 0.02 [19], essentially because of the lubrication film. These two first advantages allow one to consider that the granular structure is mainly driven by the geometrical frustrations. (iii) The grains are parallelepiped rectangles. When blocks are well ordered, the volume fraction is theoretically equal to one. On the other hand, when blocks are poured randomly in a container, the volume fraction is about 0.55 [20]. This allows a large possible range of variation for the volume fraction. (iv) The ice and the water can be easily discriminate using an x-ray tomography device. It is therefore possible to investigate the internal structure of the packing. (v) The proposed system, for which the size modification of the grains and the subsequent reorganizations, mimics the reorganization of grains that are completely surrounded by a liquid. That situation can be observed on very different scales like in ceramic science (liquid phase sintering) [20,21], metallurgy (metal scraps melting) [22], and tectonics (partial melting rocks in Earth's crust) [23].

The experimental results are first detailed according to macroscopic observables like the total volume or the total volume fraction in Sec. III A. The internal structure and the local volume fractions are then analyzed in Sec. III B. The interpretation is composed by two subsections: Sec. IV A. the ideal packing and Sec. IV B. numerical simulations.

II. EXPERIMENTAL SETUP

A cylindrical piston was built for our purpose. Its dimensions were $R_c = 75$ mm for the radius and 300 mm for the height (Fig. 1). The piston was made of a disk that can move freely in the cylinder without contact. The piston could be overweighted by the addition of a load (load 1 = 21 N, load 2 = 39 N, and load 3 = 57 N). The whole system was surrounded by polystyrene in order to decrease the exchange of heat with the exterior. The experiment duration was consequently increased and the temperature was more homogeneous through the sample. Several thermocouples were set in the system. The temperature, about -3 °C was stable during experiments and the fluctuations were below 1 °C. The thermal dilatation can be neglected as the thermal expansion of the ice is about 10^{-6}/K.

About 140 ice blocks for which dimensions were $35 \times 25 \times 25$ mm^3, were introduced in the cylinder. Two liters of cold (initially at 6 °C) salted water was added (100 g NaCl per liter). With this amount of salted water, the piston and the load are completely immersed (Fig. 1). Note that during the motion, the water located below the piston is allowed to pass on the other side of the piston. This salted liquid prevents the ice block from soldering and ensures a better thermal homogeneity of the system. Due to the buoyancy, the force exerted by the ice on the piston is estimated to 3 N, thus much lower than the load applied to the block assembly. The motion of the piston is consequently fast when the pile reorganizes.

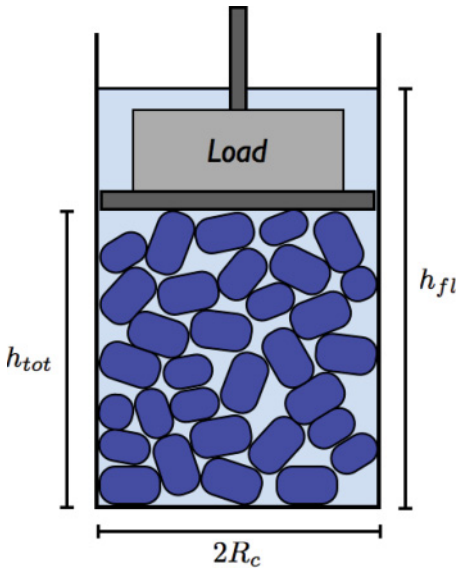

FIG. 1. (Color online) Schematic description of the experimental setup. The ice blocks bathe in salted water. They are pushed downward by the loaded piston. Two quantities are measured: the position of the piston $h_{\rm tot}$ and the variations of the liquid level h_{fl} that is related to the time variation of the volume of ice $V_{\rm ice}$ (see [4]).

The total volume was found by measuring the position $h_{\rm tot}$ of the piston with respect to the bottom. The piston without load is balanced by a counterweight using a pulley. When the piston moves, the pulley turns. A potentiometer allowed one to count the number of turns due to the motion of the piston and, after calibration, allowed to measure the position of the piston. The height $h_{\rm tot}$ was used to determine the total volume $V_{\rm tot}$ occupied by the ice, namely,

$$V_{\rm tot}(t) = \pi R_c^2 h_{\rm tot}(t). \tag{1}$$

In parallel to the total volume, we measured the ice volume by following the variations of the fluid level $h_{fl}(t)$ contained in the vessel (Fig. 1). The position of the surface was determined using a floater for which the position was measured using a proximity sensor. The melting of the ice decreases the liquid level because the blocks are completely immersed and because the density of the ice is lower than the density of the water. Knowing the position of the floater, it is possible to determine the amount of ice that melted since the beginning of the experiment. The volume $V_{\rm ice}$ of ice under the piston is given by

$$V_{\rm ice}(t) = \pi R_c^2 (h_{fl}(t) - h_{fl}(\infty)) \frac{\rho_w}{\rho_w - \rho_i},$$

where $h_{fl}(\infty)$ means "when the ice has totally melted"; $\rho_w = 1000\,{\rm kg/m^3}$, and $\rho_i = 920\,{\rm kg/m^3}$ are the density for the water and for the ice, respectively. Finally, the volume fraction η of the ice packing is defined as the ratio between the volume of ice and the total volume, namely,

$$\eta(t) = \frac{V_{\rm ice}}{V_{\rm tot}} = \frac{h_{fl}(t) - h_{fl}(\infty)}{h_{\rm tot}} \frac{\rho_w}{\rho_w - \rho_i}. \tag{2}$$

An x-ray tomography apparatus (Siemens Somatom Sensation 16) was used to determine the structure evolution of the packing. For this purpose a square vessel in plexiglas was built. The volume of interest measured $200 \times 200 \times 200$ mm^3. In this case, about 380 ice blocks of $25 \times 25 \times 20$ mm^3 was mixed with cold salted water (6 °C) in the vessel. The density contrasts between the water and the ice is such that it is possible to discriminate the ice blocks from the surrounding liquid. The volume fraction and the local density were measured during the melting process. The accessibility of these quantities allows one to characterize the internal structure of the pile [24].

III. EXPERIMENTAL RESULTS

A. Global measurements

The evolution of the total volume $V_{\rm tot}$ occupied by the assembly (red lines, left scale) and the volume fraction η (blue lines + triangles, right scale) with the time (sampling rate = 1 Hz) are represented in Fig. 2 for three loads, 21 N [Load 1, Fig. 2(a)], 39 N [Load 2, Fig. 2(b)], and 57 N [Load 3, Fig. 2(c)]. For illustration purpose, a typical experiment can be seen at Ref. [4] when the vessel is not thermally isolated. The total volume starts at about 4 dm^3. The total time for the melting is about 35 h. A dependance of the total melting time with the applied force is not observable in the present case.

The general behavior of the curves $V_{\rm tot}(t)$ is a monotonic decrease with time. The curves exhibit discontinuous variations

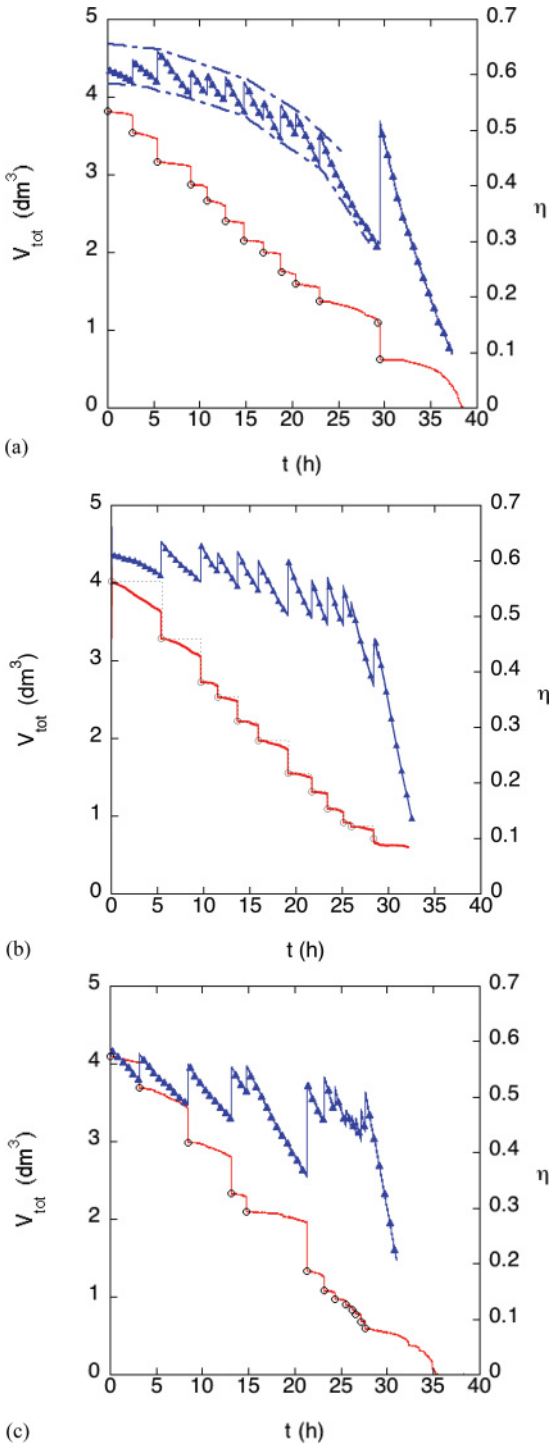

FIG. 2. (Color online) Total volume $V_{\rm tot}$ (red line) and volume fraction η (blue lines + triangles) evolutions with the time for three different loads: (a) 21 N, (b) 39 N, and (c) 57 N. The dashed curves in Fig. 2(a) represent the envelope of the volume fraction evolution with time while the dashed lines in Fig. 2(b) illustrate the variations of total volume by steps as described in the text.

during which the ice assembly shrinks and emits a loud sound. The total volume $V_{\rm tot}$ evolves by steps. The time variation of $V_{\rm tot}$ can be summed up as a succession of periods of low decreases (calm periods) separated by sudden large collapses (large discontinuities). One observes that the calm periods become longer and less regular when the load is increased. In average, a step lasts 2 h, 45 min before a breakdown occurs. The typical variation of volume due to a large discontinuity is about 5%–6% of the total initial volume (typically about 0.200 dm^3). A close look at the calm period shows that even calm periods are made of a succession of small steps [see zoom at Fig. 4(a)]. Regarding the evolution during a calm period, small discontinuities occur with a typical magnitude of 0.1% of the total initial volume (typically about 0.004 dm^3). Note that the last step ($t > 30$ h) concerns the melting of a monolayer of blocks in the piston. That explains the continuous decay of the volume fraction towards zero. At this point, the volume fraction measurement is difficult to obtain as it results from a division.

The variations of total volume $\Delta V_{\rm tot}(t) = V_{\rm tot}(t+\tau) - V_{\rm tot}(t)$ where $\tau = 1$ s (the inverse of the sampling rate) have been statistically analyzed. In order to automatically detect a discontinuity, three moving averages of $V_{\rm tot}$ were considered [25]. They are noted $\langle V_{\rm tot}(t)\rangle_n$ and defined by $\frac{1}{2n}\sum_{i=t-n}^{t+n} V_{\rm tot}(i)$. The moving averages have been computed for $n = 20$, 50, and 100. From these averages, two differential averages have been built $d_{100,20}(t) = \langle V_{\rm tot}(t)\rangle_{100} - \langle V_{\rm tot}(t)\rangle_{20}$ and $d_{50,20}(t) = \langle V_{\rm tot}(t)\rangle_{50} - \langle V_{\rm tot}(t)\rangle_{20}$. An arbitrary threshold was fixed to define a discontinuity: A discontinuity was detected when $d_{100,20}(t)$ is larger than 10^{-3} dm^3, which is about twice the value of the noise on the volume data. The time t_d at which the discontinuity occurs is found when the sign of the difference between $d_{100,20}(t)$ and $d_{50,20}(t)$ changes. The amplitude of the discontinuity ΔV_d is given by the difference between the average over the 50 values of $V_{\rm tot}$ just before and just after t_d. Finally, the time delay between two successive discontinuities is noted Δt_d.

The cumulate distribution function (CDF) of ΔV_d is reported in Fig. 3(a) and this for the three different loads. Two populations can be evidenced: (i) The small decreases ΔV_S concern total volume variations between 10^{-3} and 10^{-2} dm^3 and (ii) the collapses ΔV_H concern variations between 10^{-2} and 1 dm^3. The large collapses ΔV_H are represented by open black circles in Figs. 2(a)–2(c). The small decreases ΔV_S are observed during the calm period. The origin of the small jumps can be attributed to small reorganization but we cannot reject the hypothesis of some stick-slip of the piston. On the other hand, the distribution of the large variations ΔV_H is found to be consistent with a log-normal distribution. The averages of the distributions of ΔV_H are found to be 0.195, 0.223, and 0.283 dm^3 for the load 21, 39, and 57 N, respectively. This evidences the influence of the load that increases the average height of collapses.

In Fig. 3(b), the cumulate distribution function of the time delays Δt_d between two successive breaks is represented for the three different loads. The cutoff time is located at 200 s due to the choice of the mobile averages. However, at a first approximation, the distributions have been fitted by a Weibull function:

$$\mathrm{CDF} = 1 - \exp(-(\Delta t/\tau))^k, \qquad (3)$$

where τ is the characteristic time and k the exponent giving the shape parameter. The values of τ are 524 s, 255 s, and 344 s for the load 21, 39, and 57 N, respectively. The shape parameter is found to be around 0.8. The value of k indicates that after a

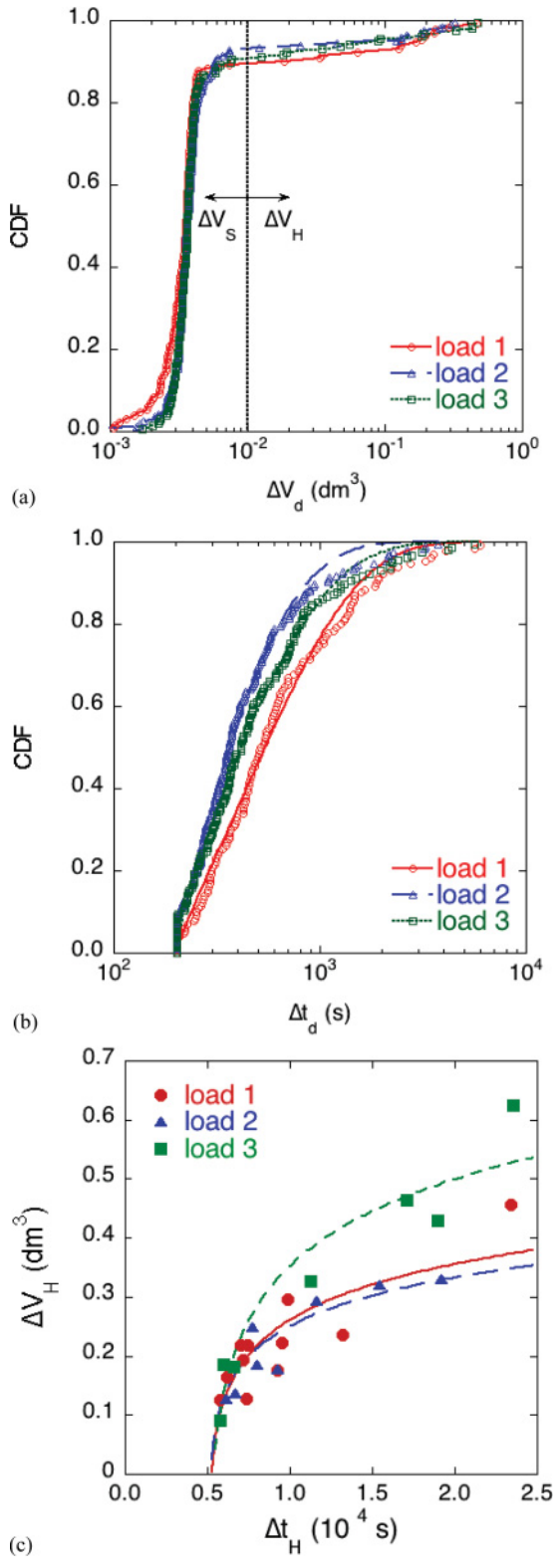

FIG. 3. (Color online) Cumulative distribution functions (CDF) of (a) the total volume discontinuities ΔV_d and (b) the time delay between two successive discontinuities for three different loads: 21 N (circles), 39 N (triangles), and 57 N (squares). (c) Correlations between the variations of the high discontinuities ΔV_H and the time elapsed Δt_H between two high discontinuities for the three different loads. The curves are guides for the eyes.

collapse, the probability of observing a new collapse decreases with time. This fact can be interpreted by considering the existence of a supporting structure through the pile (see later in the article). A jump is always due to the weakest structure present in the packing. The weak structures are the first to break. This hypothesis is well supported by the correlation found between the large collapse ΔV_H and the waiting times Δt_H between two successive large collapses. In Fig. 3(c), ΔV_H is reported as a function of Δt_H. The curves are guides for the eye. This show that a long waiting time is correlated to a high jump. A long waiting time is due to the presence of strong arches in the packing and a subsequent large reorganization is expected. The correlation between the waiting time and the amplitude of the event is typical of a "fragile medium" under a constraint and is found in numerous phenomena: self-organized critical systems [26], fracture of a solid under a constraint [27], earthquake frequency and intensity [28], bursting of bubbles in a foam [29], noise emission in geological phenomenon [30], rupture of fuse networks [31], etc.

The signal $V_{\text{tot}}(t)$ may be also decomposed into a series of steps. We define a step as the variation of the total volume at the moment just after a large collapse until the moment just after the next large collapse. Such steps are represented as a dashed line in Fig. 2(b) and a zoom is presented in Fig. 4(a). In so doing, a step is composed of a calm period during which the system shrinks nearly continuously and of a sudden decrease of the total volume. The total volume variation of a step $\Delta V_{H,\text{tot}}$, given by the difference between the total volume just after a large jump and the total volume just after the next large jump, can be decomposed into a part of nearly continuous variation and a large jump ΔV_H. In Fig. 4(b), ΔV_H is plotted as a function of the total step $\Delta V_{H,\text{tot}}$. After a linear fit, the sudden jump ΔV_H is found to be about 80% of the total step $\Delta V_{H,\text{tot}}$. Remarkably, this ratio seems to be a rule for the considered system of ice blocks. From Figs. 3(c) and 4(c), we conclude that the shape of the steps is conserved because the waiting time is correlated to the amplitude of the large collapse which is correlated to the total variation of volume during one step.

The volume fraction η of the ice contained in the considered $V_{\text{tot}}(t)$ is also plotted versus time in Fig. 2 (blue lines) in parallel with the variation of the total volume for the three loads. The initial volume fractions are situated around 0.6. That is consistent with the values found in the literature for a packing of blocks [20]. The volume fraction exhibits a saw-tooth behavior (i.e., smooth and continuous decrease periods are brutally interrupted by sudden jumps towards higher volume fractions). Indeed, during slow decrease periods, the volume of ice decreases faster than the total volume occupied by the ice blocks. It results in a decrease of the volume fraction of ice. When a sudden decrease of V_{tot} occurs, the volume fraction increases; the system gets denser. We also remark that the ice tends to occupy less and less space in the total volume as the general trend of the saw-tooth curve is to decrease with time as suggested by the envelope delimited by both dashed curves in Fig. 2(a). This also emphasizes that the load can be supported by a block assembly less and less dense.

In order to better understand the trend towards the decrease of the volume fraction, we compared the variation of the total volume $\Delta V_{H,\text{tot}}$ during one step and variation of the

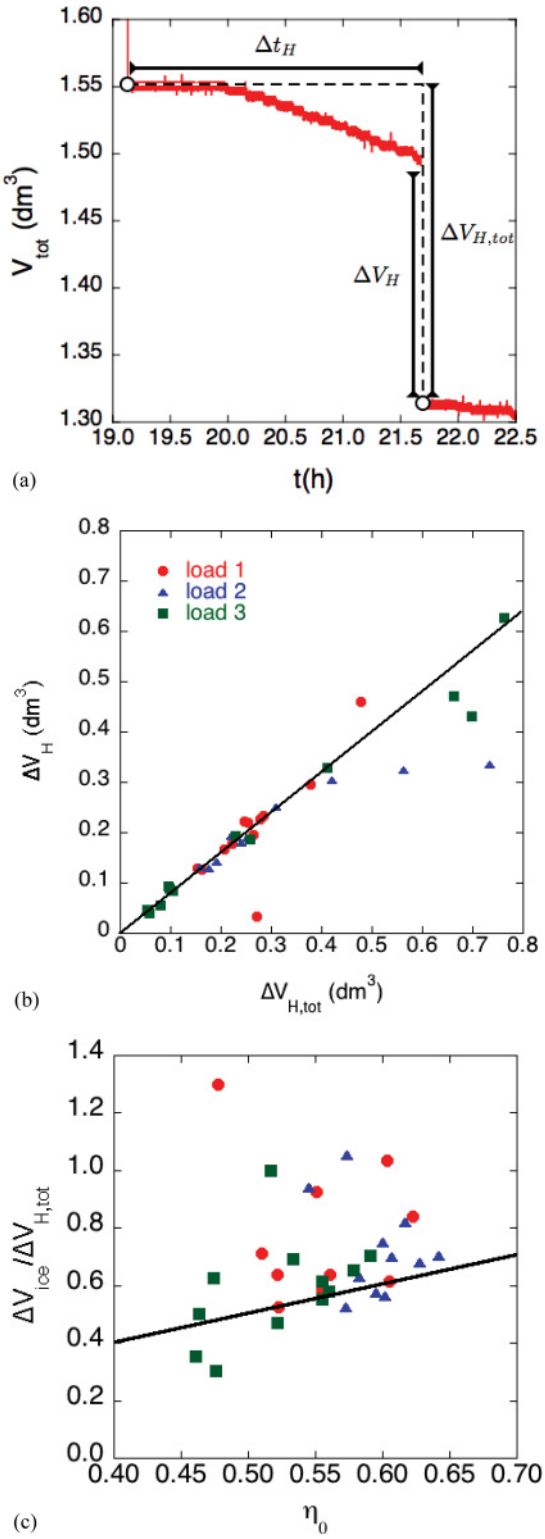

FIG. 4. (Color online) (a) During the melting, the piston experiences steps. Here is a typical step (series 39 N) for which size is $\Delta V_{H,\mathrm{tot}}$ and duration Δt_H. The contribution of the sudden jump is ΔV_H. (b) Contribution of the sudden collapse variation ΔV_H to the total variation of volume during one step $\Delta V_{H,\mathrm{tot}}$ for three loads (see legend). The line is a linear fit to the whole data presented. (c) Ratio between the variation of the ice volume during a step ΔV_{ice} and the variation of the total volume $\Delta V_{H,\mathrm{tot}}$ is represented as a function of the volume fraction η_0 measured at the beginning of a step.

ice volume ΔV_{ice} during the same period, we found that the total volume variation is, in most of the cases, larger than the ice volume variation. This fact may seem to be a paradox as a decrease trend of the volume fraction was observed. This can be explained by considering the definition of the volume fraction. Let η_0 the volume fraction just after one step at $t = t_0$. This volume fraction is given by the ratio $V_{\mathrm{ice}}(t_0)/V_{\mathrm{tot}}(t_0)$. Just after the next large collapse at $t = t_1$, the volume fraction η_1 is given by

$$\eta_1 = \frac{V_{\mathrm{ice}}(t_0) - \Delta V_{\mathrm{ice}}}{V_{\mathrm{tot}}(t_0) - \Delta V_{H,\mathrm{tot}}}. \tag{4}$$

After some basic manipulations, one finds that the value η_1 is smaller than η_0 when $\Delta V_{\mathrm{ice}}/\Delta V_{H,\mathrm{tot}} > \eta_0$. In Fig. 4(c), we report the ratio $\Delta V_{\mathrm{ice}}/\Delta V_{H,\mathrm{tot}}$ as a function of η_0. We observe that the ratio is larger than the initial value of the volume fraction in most of the cases. That clearly shows that, under a constant vertical stress, the volume fraction of a confined assembly of melting blocks naturally decreases with time. Even if large and sudden reorganizations occur, the volume fraction trend is a decrease with time.

To summarize the observations, the total volume evolves by steps. The shape of the steps can be rescaled as revealed by empirical laws which link the amplitude and the waiting time of a step. The statistical analysis of the successive steps shows that the probability of a collapse decreases with time. After several large collapses, the ice block assembly is less dense than the initial packing. However, the pile is still able to support the load.

B. Internal structure

The internal structure of a melting ice block's packing has been investigated using x-ray tomography. A three-dimensional (3D) reconstruction can be seen in Fig. 5. The x and y axes are located in a horizontal plane while the z axis is oriented along the vertical direction (for illustration, see Fig. 5). The bottom of the vessel corresponds to $z = 0$. A movie

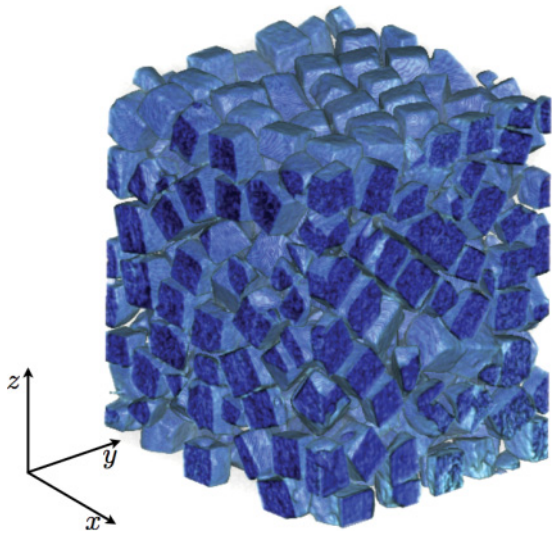

FIG. 5. (Color online) Typical 3D reconstruction of a pile of ice block by x-ray tomography (see also [4]). The size of the pile is $200 \times 200 \times 200$ mm^3.

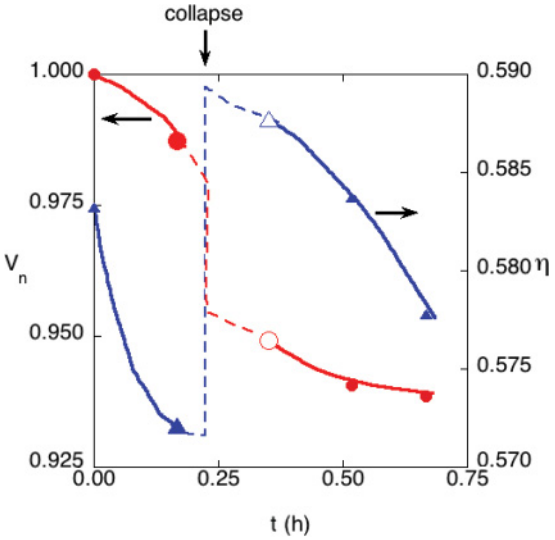

FIG. 6. (Color online) Total volume divided by the initial volume V_n (circles) and volume fraction η (triangles) evolutions with time obtained from X-tomography measurement. A re-arrangement occurs around $t \approx 0.25$ h.

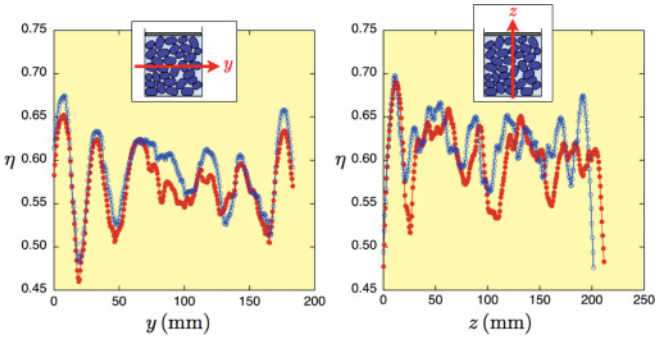

FIG. 7. (Color online) (a) Local volume fraction dependance with the horizontal coordinate y ($y = 100$ mm corresponds to the center of the vessel). (b) Local volume fraction dependance with the vertical coordinate z in the vessel ($z = 0$ corresponds to the bottom). The plain red symbols and the open blue symbols correspond to $t = 0.17$ h (before the collapse) and to $t = 0.35$ h (after the collapse).

was made using OSIRIX [32]; the movie shows the packing seen from a vertical plane that scans the whole vessel [4]. The x-ray tomography provides density maps of slices along the x axis. A scan has been performed every 10 min in order to obtain the dynamics of the melting. After thresholding the pictures using IMAGEJ [33], the volume fraction is obtained by taking the ratio between the number of pixels belonging to the ice and the total number of pixels inside the vessel. Macroscopic variables such as the total volume and the volume fraction of ice are easily deduced from image analysis. Moreover, the tomography allows one to obtain local properties like the density profile along an arbitrary direction by averaging the density of a slice orthogonal to the concerned direction.

In Fig. 6, the normalized volume $V_n = V_{\text{tot}}(t)/V_{\text{tot}}(0)$ and the global volume fraction of ice η are reported as a function of the time. The curves are arbitrary interpolations in order to recall the behaviors observed in Fig. 2. In Fig. 6, a collapse occurs between $t = 0.17$ and 0.35 h and is represented by a dashed line. Due to the collapse, the normalized volume V_n changes by about 5%. Two situations were carefully analyzed, that is, before ($t = 0.16$ h) and after the jump ($t = 0.35$ h). Both situations are indicated by large symbols in Fig. 6 (solid symbols before and open symbols after the jump).

The density profiles were calculated along two orthogonal directions, namely y and z, and are presented in Figs. 7(a) and 7(b), respectively. For each direction, two situations are analyzed, namely before (plain red circles) and after (open blue circles).

In Fig. 7(a), the density profile along the y axis is reported. On the measurements before and after the collapse, large oscillations can be observed close to the walls. This reflects that the grains are ordered along the walls. Moreover, the volume fraction is found to be the largest along the wall. That strongly contrasts with the center of the pile which is less dense and less organized. It is noticeable that after the collapse, the oscillation amplitude of the density profile increased. Due to the reorganization, the grains located along the walls becomes more organized.

According to the vertical z axis [Fig. 7(b)], the curves corresponding to the density profile before and after the jump present oscillations close to the bottom (close to $z = 0$ mm). This shows that the pile is rather well organized in layers at the bottom. After the collapse, the total height of the pile decreases by about 10 mm as can be seen in Fig. 7(b) (close to $z = 200$ mm). Larger oscillations of the density profile are observed close to the top of the pile (open circles).

From the local density profiles, we observe that the blocks are organized along vertical layers that are located along the wall of the container. Note that such an organization is also found in the case of spheres (experimentally [34] and numerically [35]) and in the case of ellipsoid grains [36]. This structure is a signature of the confinement of the granular material, in other words when the size of the grains are comparable to the size of the container. The local volume fraction is also the largest along the vertical walls and at the bottom of the container while the center of the pile is the less dense. After the collapse, the pile becomes even better organized and denser along the walls, at the bottom and at the top while the center remains not organized and less dense. The structure of the ice block assembly evolves toward a dense and organized shell of blocks that surrounds a not well-organized and less dense core of blocks.

IV. INTERPRETATION

From these observations, it is possible to establish a scenario for the evolution of the melting granular material under an external constraint. As for any noncohesive granular material, the stability of the pile is ensured by the geometrical frustration and by the friction between the grains. In the case of ice blocks, the geometrical frustration is the predominant mechanism for the generation of arches as the block-block friction is very low. When the grains (ice blocks) melt, they occupy less and less space; their shape becomes rounded. Consequently, the geometry of the contact network reorganizes. The experimental facts evidence that two kinds of reorganization processes may occur. In the first one, called

the calm period, small jumps may be observed. The grains are melting; the change of ice volume is faster than the change of total volume. Consequently, the volume fraction decreases with time. The reorganization of the contact network is supposed to be continuous or at least very smooth during calm periods. The second reorganization process corresponds to the sudden collapses. Within a second, the total volume drops. A noise can be heard. Macroscopic motion of ice blocks can be observed [4]. As the ice volume remains constant during the breakdown, the volume fraction increases. The reorganization is discontinuous. We showed that the total volume evolves by successive steps. This fact does not seem to be influenced by the value of the load. This suggests again that the geometrical structure of the pile plays a key role in the reorganization process. Regarding the internal structure, we evidenced that the blocks are better organized along the walls as the density is larger. These blocks form a dense envelope around a less dense core of blocks. As the friction between the grains is very low, we may surmise, as a first approximation, that the pile is more resistant to the load when it is well ordered (i.e., along the walls). Even if the blocks geometry is rather complex as the grains are rounded polyhedrons, these particular blocks can be seen as a two-dimensional (2D) vertical structure.

As mentioned, the geometry of the packing plays an important role as the friction between the grains is very low. Moreover, as the size of the blocks are about one-tenth of the size of the container and as the piston goes downward, the confinement plays also a key role. First of all, when the size of the blocks and the size of the container are not commensurable, topological defects are generated and this even if spheres are envisaged. As the grains are melting, their size continuously decreases but also the total volume of the container. We showed that (i) the total volume decreases faster than the total volume of ice [$\Delta V_{\text{ice}}/\Delta V_{H,\text{tot}} < 1$; Fig. 4(c)] and (ii) the volume fraction is found to globally decrease with time (Fig. 2). That indicates that the confinement increases with time. This is supported by the numerical simulation of confined granular material by Desmond *et al*. [37].

In the following, as a first step towards the description of the melting of a granular assembly, we consider a 2D system. First, we discuss the melting of an ideal infinite, frictionless packing of disks. Afterwards, using numerical simulations based on molecular dynamics, we investigate the behavior of a pile of disks constrained under a load. Two cases will be discussed: when the friction is equal to 0.8 and when the friction is null. The numerical simulation approach allows one to evidence the role of the friction and of the confinement. We will show that the reduction to a 2D grain assembly constitutes a heuristic and fruitful system.

A. Ideal melting packing

Let us start from a hexagonal lattice of disks of radius r, $r = R$ being the initial value of the radius [Fig. 8(a)]. The pile is made of a succession of disk layers, numbered from 1 to 4 in Fig. 8 (No. 1 is the lowest layer). We grayed the layers Nos. 1 and 3 to better visualize the layers. We define a cell of the lattice that contained three particles. The width w and the height h_c of the cell are equal to $2R$ and to $3\sqrt{3}R$, respectively. Such a cell is represented by a rectangular box in Fig. 8(a). The

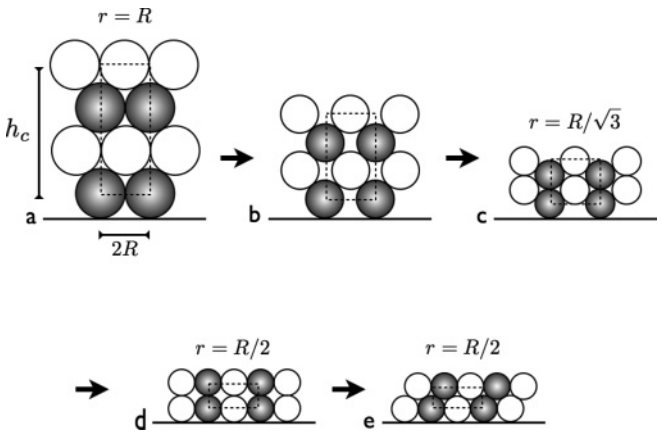

FIG. 8. Evolution of the hexagonal lattice of disks when the radius r of the disks are decreased. (a) $r = R$, (b) $R > r > R/\sqrt{3}$ ($r = R/\sqrt{2}$ corresponds to a tilt square lattice), (c) $r = R/\sqrt{3}$ (tilt hexagonal lattice), (d) $r = R/2$ (square lattice), and (e) $r = R/2$ (hexagonal lattice).

surface fraction η_c of disks is given by $\eta_c(r = R) = \pi/2\sqrt{3} \approx 0.907, \ldots$.

The radius r of the disks is then continuously decreased keeping constant the horizontal coordinates of the center of mass of the disks and keeping the pile mechanically stable. Consequently, the width w of the cell remains constant at $w = 2R$. On the other hand, the height h_c and the surface fraction η_c depend on the ratio $x = r/R$. On Fig. 8(b), we present the situation when r has been slightly decreased. Two particular radii r have to be taken into account: (i) when $r = R/\sqrt{3}$, the layers Nos. 1 and 3 are in contact [Fig. 8(c)] and (ii) for a radius just below $r = R/2$, the lattice becomes mechanically unstable and the lattice switches from a square to a hexagonal lattice [Figs. 8(d) and 8(e)]. The height h_c of the cell and the surface fraction η_c are given by

$$\begin{aligned} R > r > R/\sqrt{3} \quad & h_c = 3\sqrt{4r^2 - R^2}, \\ & \eta_c = \pi r^2/\sqrt{4r^2 - R^2}, \\ R/\sqrt{3} > r > R/2 \quad & h_c = 2r + \sqrt{4r^2 - R^2}, \\ & \eta_c = \pi r/(2R). \end{aligned}$$

These equations are plotted in Fig. 9. The continuous curve (red) and the continuous curve decorated with triangles (blue) correspond to the evolution of h_c/R and η_c, respectively, with the ratio x. The minimum of $\eta_c(x)/R$ is due to the fact that the squared (tilted) lattice is obtained when $x = \sqrt{2}/2$. The maximum is obtained when the lattice is hexagonal, $x = 1$ and $x = \sqrt{3}/3$ (the lattice is tilted). A sudden transition occurs at $x = 0.5$. The lattice transits from a squared lattice to a hexagonal one. The height of the cell drops at about 15%. On the other hand, the surface fraction jumps from the surface fraction of the squared lattice $\eta_c = \pi/4$ to the one of the hexagonal lattice $\eta_c = \pi\sqrt{3}/6$. After this reorganization, the pile evolves in a similar way. The step shape is conserved.

This basic model exhibits the main features observed in the dynamics of the melting ice block assembly. (i) The evolution of V_{tot} and h_c is continuous during the melting of the blocks. (ii) The curvatures of the total volume evolutions $V_{\text{tot}}(t)$ is

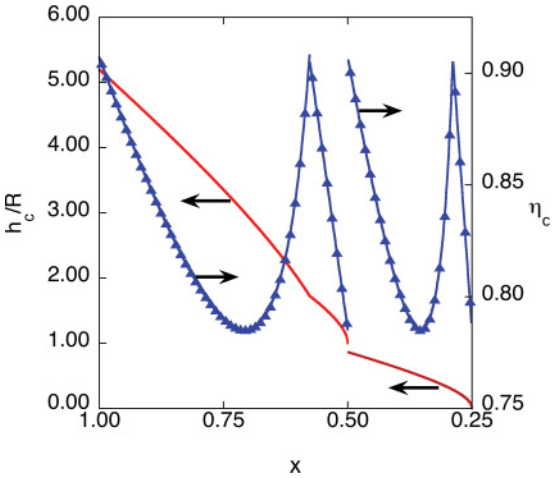

FIG. 9. (Color online) Calculated variation of the height h_c/R (continuous red curve) of a lattice cell and the surface fraction of disks η_c (continuous blue curve decorated with triangles) placed in a hexagonal close-packed configuration due to the decrease of the disk size reduction factor x.

the same as $h_c(x)$. (iii) A discontinuity occurs. (iv) The step shape is conserved. (v) The surface fraction evolves in saw teeth. To sum up, the evolution of the ideal packing due to the melting is governed by the evolution of the lattice: hexagonal $\rightarrow$ tilt square $\rightarrow$ tilt hexagonal $\rightarrow$ square which is unstable and should collapse into an hexagonal lattice again.

Three remarks should also be pointed out. First, let us recall that in the experiment, the shape of the grains is complex and far from the ideal sphere or disk. Moreover, a block located along a wall may also be ejected from the layer. However, the model reproduces pretty well the main observations. Secondly, the probability of rearrangement was experimentally found to decrease with time [Fig. 3(b)]. The origin of this behavior has been related to confinement effects [37]. Third, a similar argument applies to an ideal 3D system of melting spheres. However, the story is different whether we start with a hexagonal close-packed (HCP) or a face-centered cubic (FCC) lattice. Starting from an HC packing, when the size of the spheres decreases, the lattice evolves to a stack of aligned graphenelike plane of spheres. As the grains are vertically aligned, the structure becomes unstable and collapses. The situation after collapse is less clear than in the 2D system. On the other hand, starting from an FCC structure, the assembly evolves toward a cubic lattice which is unstable and collapses toward an HC or an FCC structure.

B. Numerical simulations

On the basis of the observations and of the theoretical considerations about the melting of an assembly of disks, numerical simulations were performed in order to capture the role of the confinement and of the friction in a 2D assembly constrained in a piston. The numerical simulations are based on a molecular dynamics algorithm described in more detail in Refs. [38–40].

In the simulation, $N = 1000$ disks of initial radius R were dropped in the piston for which the width is about $60R$. For the initialization of the packing, the disks are randomly distributed

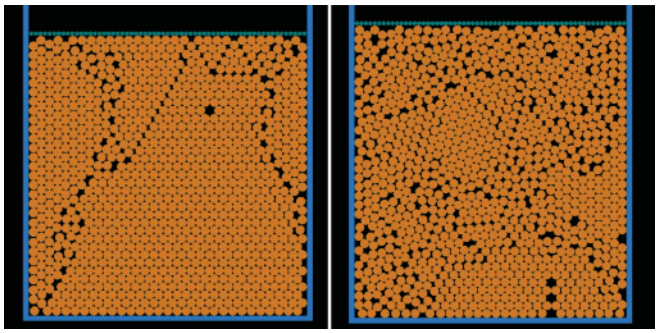

FIG. 10. (Color online) Numerical simulations are as follows: initial configuration of the packings (left) $\mu = 0$ and (right) $\mu = 0.8$. The piston is the green layer of grains at the top.

in the box avoiding any contact. The disks are then released and arranged at the bottom of the box under the action of the gravity. Their positions are the ballasted piston which sets the upper limit of the pile at about twice the weight of the grains. We compare the melting behavior for two values of the friction μ between the beads (i.e., $\mu = 0$ and $\mu = 0.8$). Starting with disks of radius $r = R$, the radius r of the disk is continuously decreased until $r = R/2$. A simulation step lasts until the pile is at the equilibrium. Knowing the position of the piston, it is very easy to determine the total volume V_n normalized by the total volume when $r = R$ and the surface fraction η.

In Fig. 10, both initial situations ($r = R$) are represented. On the left, the friction is zero while in the picture on the right, the friction μ equals 0.8. By comparison, the frictionless pile is much more crystallized than with friction. Large hexagonal arrangement domains can be observed. On the other hand, the pile obtained with friction is characterized by numerous defects. Consequently, the total volume of the initial situation is larger in the friction case.

The origin of the defects is different whether the friction is considered or not. In the frictionless case, the confinement and the incommensurability between the grains and the vessel generate defects which geometrically propagate through the whole pile. On the other hand, the friction sculptures arch across the assembly. These structures deviate the vertical weights of the disks towards the wall (Jansen effect). The force network is then inhomogeneous and the surface fraction lowered.

At the following link [4], a movie of the melting of the disks can be seen in both situations ($\mu = 0$ and $\mu = 0.8$). In the frictionless case, the defects are very mobile and start from the walls (when the grain size is incommensurable with the size of the vessel). On the other hand, when the friction is not negligible, the "motion" of the defect is rather smooth. They disappear during the melting. In Figs. 11(a) and 11(b), the normalized volume V_n and the surface fraction η are plotted as a function of the evolution of the disk radius r normalized by the initial radius R. The general behavior of the normalized volume is a monotone decrease in both cases. However, in the frictionless case, V_n decreases by a succession of steps. In Figs. 11(c) and 11(d), two zooms of Fig. 1(a) are proposed in order to show the steps. The behavior of V_n in the friction case is smoother.

The contrast between the behavior of the melting with and without friction is more revealed by the evolution of the surface

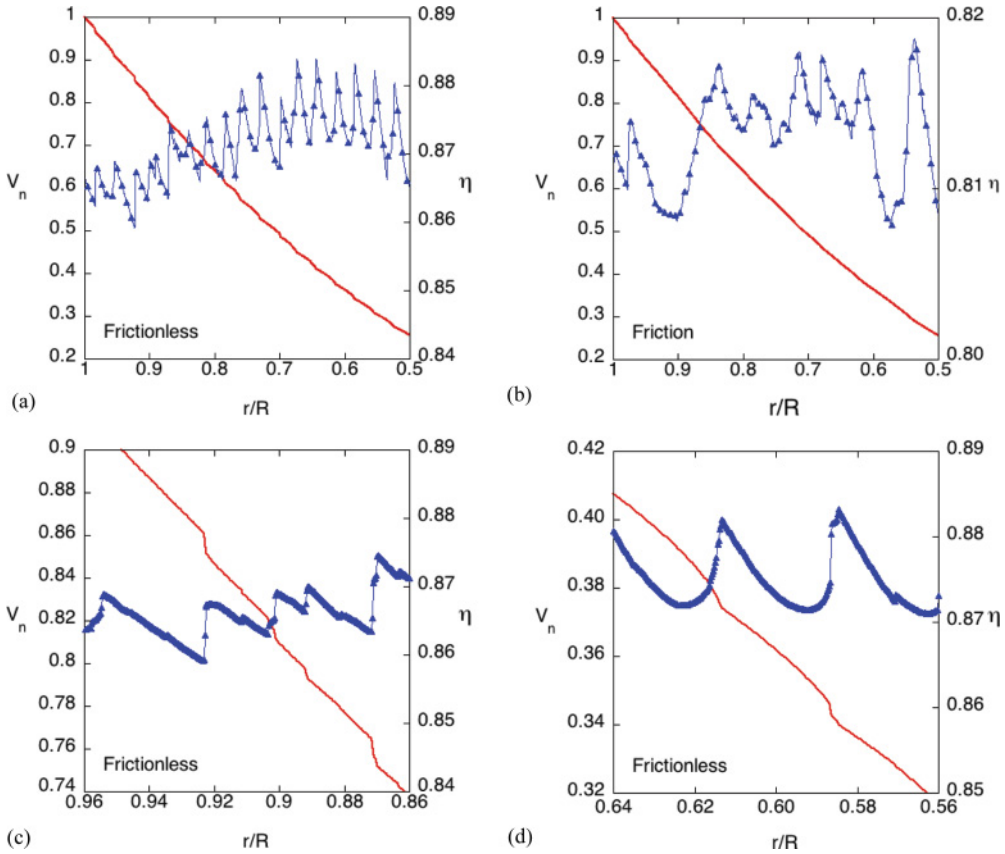

FIG. 11. (Color online) Evolution of the normalized volume V_n of the pile under the piston (red curves) of the surface fraction η (blue curves) as a function of the radius of the disks r normalized by the initial size of the disks R. (a) $\mu = 0$, (b) $\mu = 0.8$, (c) and (d) zooms of Fig. 11(a).

fraction. In the frictionless case, the surface fraction evolves as a regular saw tooth. At the beginning (when the grains are the largest compared to the size of the vessel, jumps in both V_n and η can be observed) [Fig. 11(a)]. The jumps evidence the sudden reorganization of the packing when a defect disappears. The behavior becomes more "periodic" for smaller values of r and reminds one of the ideal behavior found in Fig. 9 and the experimental results in Fig. 2. When the friction does play a role, the surface fraction evolves irregularly which strongly contrasts with the frictionless case. That suggests that for large load, the friction between the ice blocks starts to play a role. This is pretty clear when comparing the regular behavior of the volume fraction in Fig. 2(a) for a 21-N load and the irregular behavior in Fig. 2(c) for a 57-N load.

The theoretical systems that we considered here (ideal packing and numerical simulations) do not include the shape modification of the grains due to the melting and are only 2D. However, they contain enough physical ingredients to reproduce the continuous and discontinuous variations of both the total volume and the volume fraction. Moreover, these basic approaches allowed one to evidence the role of the friction and of the confinement.

V. CONCLUSION

We investigated the behavior of a granular pile under an external vertical constraint (the load) while the grains are melting. The total volume occupied by the blocks decreases by successive steps. The total volume decreases continuously until a sudden large collapse occurs. The time duration and the amplitude of the steps are correlated which shows that the steps may be rescaled. In parallel, the volume of the ice was measured which allowed one to evaluate the volume fraction of the ice in the packing. The volume fraction exhibits saw-teeth behavior because of the sudden collapse of the total volume. However, the volume fraction observed after a collapse decreases after several steps. X-ray tomography was performed in order to investigate the internal structure of the ice block pile. The grains are organized and the density profile is high along the wall. After a collapse, the layers are denser and better organized than before, even at the bottom and at the top of the pile. Consequently, after several collapses, the structure of the pile may be pictured as a dense and organized "crust" of ice blocks that surrounds a less organized and less dense core.

Because the friction between the blocks is very low, we suggest that the ordered part of the assembly (the grains along the walls) is responsible for the stability. The layer along the wall has been modeled by a 2D pile of disks for which radii decreases continuously (shape-invariant model). We investigated (i) a perfect 2D packing of melting disks (calculations) and (ii) confined 2D disk packing with and without friction (simulations). The perfect 2D packing is able to reproduce qualitatively these observations: (i) continuous and sudden reorganizations and (ii) the amplitude of the step is

related to the waiting time between two steps. The simulations allowed one to lighten the role played by the confinement which generates defects through the 2D frictionless disk's assembly. During the melting, discontinuities in the volume fraction are observed. They are due to (i) the discontinuous transition between a hexagonal and square lattice and (ii) to the disappearance of defects. The observed behaviors are essentially due to confinement effects and to the low friction between the ice blocks. This work also suggests investigating in detail the role of the confinement on 2D structures.

ACKNOWLEDGMENTS

S.D. thanks Le Fonds de la Recherche Scientifique (FNRS) for financial support. B. Wiesen is warmly acknowledged for the help in the technical setup devoted to x-ray tomography. J. Y. Remy is especially thanked for the realization of the square vessel. J.Y. Raty is thanked for his help with 3D figures. Finally, the authors thank Professors B. Vertruyen (ULg), J. Vander Auwera (ULg), and J. Lecomte (ULg) for fruitful discussions.

[1] S. Torquato, T. M. Truskett, and P. G. Debenedetti, Phys. Rev. Lett. **84**, 2064 (2000).
[2] S. Torquato and F. H. Stillinger, Rev. Mod. Phys. **82**, 2633 (2010).
[3] A. Janda, D. Maza, A. Garcimartin, E. Kolb, J. Lanuza, and E. Clément E, Europhys. Lett. **87**, 24002 (2009).
[4] See Supplemental Material at http://link.aps.org/supplemental/10.1103/PhysRevE.xx.xxxxxx for movies of the melting ice assembly, the reconstruction of a pile by x-ray tomography, and the simulations.
[5] O. Dauchot, Lect. Notes Phys. **716**, 161 (2007).
[6] A. Donev, I. Cisse, D. Sachs, E. A. Variano, F. H. Stillinger, R. Connelly, S. Torquato, and P. M. Chaikin, Science **303**, 990 (2004).
[7] A. Donev, F. H. Stillinger, P. M. Chaikin, and S. Torquato, Phys. Rev. Lett. **92**, 255506 (2004).
[8] J. Baker and A. Kudrolli, Phys. Rev. E **82**, 061304 (2010).
[9] J. B. Knight, C. G. Fandrich, C. N. Lay, H. M. Jaeger, and S. R. Nagel, Phys. Rev. E **51**, 3957 (1995).
[10] P. Philippe and D. Bideau, Europhys. Lett. **60**, 677 (2002).
[11] G. Lumay and N. Vandewalle, Phys. Rev. Lett. **95**, 028002 (2005).
[12] F. Ludewig, S. Dorbolo, T. Gilet, and N. Vandewalle, Europhys. Lett. **84**, 44001 (2008).
[13] P. Richard, M. Nicodemi, R. Delannay, P. Ribière, and D. Bideau, Nature Mater. **4**, 121 (2005).
[14] M. Nicolas, P. Duru, and O. Pouliquen, Eur. Phys. J. E **3**, 309 (2000).
[15] J. Zhang, T. S. Majmudar, A. Tordesillas, and R. P. Behringer, Gran. Mater. **12**, 159 (2010).
[16] T. Divoux, H. Gayvallet, and J. C. Geminard, Phys. Rev. Lett. **101**, 148303 (2008).
[17] E. Kolb, C. Goldenberg, S. Inagaki, and E. Clément, J. of Stat. Mech. (2006) P07017.
[18] B. Turnbull, Phys. Rev. Lett. **107**, 258001 (2011).
[19] F. P. Bowden and T. P. Hughes, Proc. R. Soc. A **172**, 462 (1953).
[20] M. N. Rahaman, *Ceramic Processing and Sintering*, 2nd ed. (Marcel Dekker, New York, 2003).
[21] R. M. German, P. Suri, and S. J. Park, J. Mater. Sci. **44**, 1 (2009).
[22] D. Guo and G. A. Irons, Appl. Math. Model. **32**, 2041 (2008).
[23] M. S. Paterson, Tectonophys. **335**, 51 (2001).
[24] P. Richard, P. Philippe, F. Barbe, S. Bourlès, X. Thibault, and D. Bideau, Phys. Rev. E **68**, 020301(R) (2003).
[25] N. Vandewalle and M. Ausloos, Phys. Rev. E **58**, 6832 (1998).
[26] R. Sanchez, D. E. Newman, and B. A. Carreras, Phys. Rev. Lett. **88**, 068302 (2002).
[27] A. Garcimartin, A. Guarino, L. Bellon, and S. Ciliberto, Phys. Rev. Lett. **79**, 3202 (1997).
[28] A. Saichev and D. Sornette, Phys. Rev. Lett. **97**, 078501 (2006).
[29] N. Vandewalle, J. F. Lentz, S. Dorbolo, and F. Brisbois, Phys. Rev. Lett. **86**, 179 (2001).
[30] G. Niccolini, A. Carpinteri, G. Lacidogna, and A. Manuello, Phys. Rev. Lett. **106**, 108503 (2011).
[31] D. Sornette and C. Vanneste, Phys. Rev. Lett. **68**, 612 (1992).
[32] http://www.osirix-viewer.com/.
[33] [rsbweb.nih.gov/ij/].
[34] G. T. Seidler, G. Martinez, L. H. Seeley, K. H. Kim, E. A. Behne, S. Zaranek, B. D. Chapman, S. M. Heald, and D. L. Brewe, Phys. Rev. E **62**, 8175 (2000).
[35] J. W. Landry, G. S. Grest, L. E. Silbert, and S. J. Plimpton, Phys. Rev. E **67**, 041303 (2003).
[36] W. N. Man, A. Donev, F. H. Stillinger, M. T. Sullivan, W. B. Russel, D. Heeger, S. Inati, S. Torquato S, and P. M. Chaikin, Phys. Rev. Lett. **94**, 198001 (2005).
[37] K. W. Desmond and E. R. Weeks, Phys. Rev. E **80**, 051305 (2009).
[38] S. Luding, Gran. Matt. **10**, 235 (2007).
[39] L. Silbert, D. Ertas, G. Grest, T. Halsey, and D. Levine, Phys. Rev. E **65**, 031304 (2002).
[40] E. Opsomer, F. Ludewig, and N. Vandewalle, Phys. Rev. E **84**, 051306 (2011).